Hydrothermal $BaTiO_3$ thin films from nanostructured Ti templates

Hasan Akyıldız
Department of Metallurgical and Materials Engineering, Middle East Technical University, 06531 Ankara, Turkey
Michelle D. Casper, Seymen M. Aygün, Peter G. Lam, and Jon P. Maria[a)]
Department of Materials Science and Engineering, North Carolina State University, Raleigh, North Carolina 27606

(Received 20 July 2010; accepted 9 November 2010)

Polycrystalline $BaTiO_3$ thin films have been prepared by hydrothermal reaction with sputter-deposited nanostructured reactive Ti templates designed to control net diffusion direction and distance. Templates were prepared in two morphologies, i.e., planar and nanopillar. The samples produced from flat templates showed sluggish transformation kinetics and an eventual termination of reaction without fully consuming the Ti metal. Templates with pillar morphology, on the other hand, could be transformed to phase-pure $BaTiO_3$, independent of the template thickness. In the as-precipitated state, those films revealed a permittivity of ~1000 and loss tangent values around 0.1 with mild dispersion in the kilohertz frequency range. Annealing these films under forming gas containing 1 vol% H_2 balance N_2 for 3 h at 200 °C decreased high-field losses to 0.06 and reduced dispersion. Mn incorporation as an in situ acceptor dopant was also explored. Addition of Mn during hydrothermal treatment further improved the electrical properties. Annealing under the same postgrowth conditions virtually eliminated the frequency dispersion in the range of 1 kHz to 1 MHz, while maintaining permittivity values in the range of 350.

I. INTRODUCTION

Complex oxide ceramics with high-performance electrical properties are in demand for a range of electronic applications. Among them, $BaTiO_3$ has received much attention as a multilayer ceramic capacitor, a nonlinear resistor, and a varactor (voltage-controlled capacitors) due to its high permittivity and nonlinear ferroelectric response.[1–2] A variety of deposition techniques have been used for the production of $BaTiO_3$ thin films, such as metal-organic chemical vapor deposition,[3] sputtering,[4] pulsed laser deposition,[5] electrochemical deposition,[6] sol–gel,[7] spray-pyrolysis,[8] and chemical solution deposition.[9] However, most of these techniques require exposure to high temperatures for complete crystallization and organic removal. In some cases, this high-temperature annealing can promote inhomogeneous film composition, porosity, cracking, or peeling of the deposited films.[10] Further, it presents severe limitations for the integration of ferroelectrics on printed wiring boards or other organic substrates.[11]

Hydrothermal processing has evolved over the last three decades and provides the opportunity of direct synthesis of crystalline structures at significantly lower temperatures[12–16] in strong alkaline solutions. Films of $BaTiO_3$ were precipitated on Ti-coated polyphenylene sulfide,[12] silicon,[10,17–24] platinized silicon,[25] printed circuit board,[26] FR4 Cu-clad laminates,[11] kapton tape,[16] and pure and anodized Ti-foils or plates[27–30] by utilizing hydrothermal techniques. In all studies, planar Ti films were deposited and utilized as a precursor. According to those studies, the formation of $BaTiO_3$ films by hydrothermal process depends on a dissolution–precipitation reaction.[22,29,31,32] This mechanism requires dissolution of Ti from the template into the solution and then precipitation of $BaTiO_3$ when the supersaturating value is reached. Nucleation and growth of a $BaTiO_3$ layer on top of the template inhibits further dissolution of Ti and limits the final thickness of the ceramic layer.[22] In addition, the compositions of the films are not homogenous, as there is no clear interface separating the template and the film,[33,34] which brings difficulties when interpreting electrical measurements. It has been demonstrated experimentally that extending the reaction time, increasing the concentration of $Ba(OH)_2$, or increasing the temperature did not increase the precipitating layer thickness without limit or consume the entire Ti layer.[19] Further, if the reactive Ti template is thinned to a level that enables full consumption, complete dissolution will occur and a continuous $BaTiO_3$ film will not deposit on the parent substrate. Thus, complete conversion of the precursor layer to the ceramic film under consideration is an important concern.

It is well known that the hydrothermal processing produces a defective structure, such as proton incorporation due to hydroxyls entrapped in the lattice and on the surface of the film.[13,14,23,30,35] As expected, protons have an adverse effect on the dielectric properties of $BaTiO_3$

[a)]Address all correspondence to this author.
e-mail: jpmaria@ncsu.edu
DOI: 10.1557/jmr.2010.102

 © Materials Research Society 2011

https://doi.org/10.1557/jmr.2010.102 Published online by Cambridge University Press

thin films.[36] High-dielectric constant values observed in as-precipitated films are in many cases attributed to additional polarization mechanisms that operate at radio frequencies, with relaxation times related to hydroxyl group contributions.[35] Similarly, high dielectric loss of the films depends on the time lag between the hydroxyl dipole switching rate and migration losses due to proton hopping.[26] A postannealing treatment is generally accepted to be useful for eliminating point and line defects in those films.[16,35,36] It is reported that annealing under nitrogen below 250 °C could remove bonded H_2O and OH^- only from the film surfaces.[14] The need of higher temperatures was reported to remove all the lattice hydroxyls.[35] Incorporating acceptor dopants during synthesis could be an alternative or a supporting mechanism to postannealing, similar to charge compensation observed in $BaTiO_3$ thin films processed under low pO_2 conditions, as in the cases of addition of Mn, Mg, and Ca ions.[37] Those largely immobile aliovalent ions can help to reduce and compensate the defects formed inevitably when processing $BaTiO_3$ in basic aqueous media at low temperatures. In a study,[38] following a similar idea, the effects of Mg-doping on the electrical properties of hydrothermally produced $BaTiO_3$ powders were discussed. It was shown that Mg substantially occupied *B*-sites, and the optimized ratio of Mg/Ti was found as 0.06 for high-dielectric constant and a high-breakdown electric field.

In this article, we demonstrate that by controlling the delivery and spatial distribution of precursor chemicals at the nanometer scale, low temperature reactions can be used to fabricate thin-layer microstructures that exhibit greater uniformity and higher density than by conventional hydrothermal precipitation. By delivering precursors and initiating reactions with spatial distribution comparable to the final crystalline phase, deposition times are reduced, thicker layers can be grown, and the need for long-range diffusion is minimized. We are also reporting the effects of in situ acceptor doping during hydrothermal transformation and postannealing under forming gas on the electrical properties of the films.

II. EXPERIMENTAL PROCEDURE

A. Template production

The Ti templates were prepared in two complementary film geometries, i.e., planar and pillar. They were RF magnetron sputtered on Si and platinized-Si wafers from a 2-inch diameter Ti target. Pure argon was used as the sputtering gas with a deposition pressure of 1 mTorr. Planar templates were deposited at a 4.9-W/cm^2 target power density for deposition times resulting in Ti films with 50, 100, 200, 250, 400, and 500 nm thickness values. Target to substrate separation distance was 12.5 cm for those templates. Pillar type films, on the other hand, were produced via collimated glancing angle sputter deposition. Identical sputtering conditions were used as mentioned earlier, except the angle between the substrate normal and the target was set to 85° to obtain pillar morphology as has been discussed in detail elsewhere.[39] Base pressure was maintained at ~1×10^{-7} mTorr prior to all depositions.

B. Hydrothermal synthesis

Thin films of $BaTiO_3$ were produced hydrothermally in a pressure vessel by reacting those Ti templates with Ba^{2+} ions in a highly alkaline solution. The initial solution was prepared by dissolving $Ba(OH)_2$ in boiling distilled water. The effect of Ba concentration on transformation was examined by preparing solutions with concentrations of 0.5, 1.0, and 1.5 M. In some experiments, 0.1 M KOH was added as a mineralizer to enhance the precipitation efficiency. Two or three pieces of templates were placed at the bottom of an empty Teflon liner. The premixed Ba solutions were added to the reaction vessel by straining through filter paper once the solution premix cooled to room temperature. The final volume of the alkaline solution added to the vessel in each case was 50 mL. The reaction vessel was sealed and ramped to the desired dwell temperature at a heating rate of 3 °C/min. Films were maintained under hydrothermal conditions at 200 °C for 2, 5, 10, 15, 20, and 24 h. Experiments were carried out under a pressure of 16 bar. This is the saturated vapor pressure of water at the temperature of 200 °C. Where Mn-doping was explored, separate dopant precursor solutions were prepared by dissolving 0.036, 0.072, 0.109, 0.145, and 0.218 g $MnCl_2 \cdot 4H_2O$ in 5 mL boiling distilled water and filtering upon cooling of the solution. These saturated Mn-precursor solutions were added into the $Ba(OH)_2$ solution to provide concentrations of 0.5, 1.0, 1.5, 2.0, and 3.0 at.% Mn. The amount of Mn-doping was predicted based on the Ba content in the primary solution. For all depositions, the reactor was opened after cooling to 50 °C following the hydrothermal step. The samples were rinsed with methanol and washed ultrasonically in hot distilled water for 30 sec to remove the possible carbonates remaining on the film surface. Finally, the films were dried under ambient conditions overnight on a hot plate surface maintained at 100 °C.

After drying, 250-nm thick Pt top electrodes were DC magnetron-sputtered to complete the metal–insulator–metal stack. Depositions were performed at 3.7 W/cm^2 in an Ar pressure of 30 mTorr, through a shadow mask. Postannealing was carried out in a tube furnace at 200 °C for 3 h under different atmospheres, i.e., ambient conditions, flowing O_2 and forming gas containing 1% H_2 balanced with N_2, through a room-temperature water bubbler.

Phase identification of templates and as-precipitated samples was performed by x-ray diffraction (XRD) using a Bruker AXS D5000 4-circle diffractometer equipped with a HighStar area detector (Bruker AXS, Madison, WI). Cu K_α radiation was used as an x-ray source and operated at 40 kV and 30 mA. X-rays were delivered through a

https://doi.org/10.1557/jmr.2010.102 Published online by Cambridge University Press

0.8-mm diameter circular collimator. The film-surface topography and microstructure were characterized by atomic force microscopy (AFM) using a Nanosurf Easyscan 2 (Nanoscience Instruments, Phoenix, AZ) operated in tapping mode and by field-emission scanning electron microscopy (FE-SEM) with JEOL 6400F instrument (JEOL Ltd, Tokyo, Japan). Film thickness was measured by using Dektak 150 surface profiler (Veeco, Plainview, NY) and FE-SEM. Capacitance and dielectric loss were measured with a Hewlett-Packard 4192A Impedance Analyzer (Agilent Technologies, Santa Clara, CA). Capacitance-density versus frequency curves were plotted at zero DC bias with oscillator amplitude of 0.05 V and frequency in the range of 100 Hz to 1 MHz.

III. RESULTS AND DISCUSSION

A. Flat templates

Figure 1 shows XRD data for $BaTiO_3$ layer formation on planar Ti films as a function of reaction time and solution molarity. An as-deposited pattern of the Ti template is also given as a comparison in both graphs. Figure 1(a) was obtained by treating 250-nm thick Ti films in a 1.5-M solution at 200 °C for 5, 10, and 15 h. The x-ray pattern after 5 h of reaction reveals the formation of $BaTiO_3$. On the other hand, there are still intense peaks belonging to Ti after 15 h of hydrothermal reaction, indicating only partial transformation to $BaTiO_3$. Similarly, Fig. 1(b) shows x-ray data obtained from 500-nm thick Ti films treated for 5 h at 200 °C in solutions with concentrations of 1.0 and 1.5 M and also in a 1.5-M solution containing 0.1-M KOH mineralizer. The intensities of $BaTiO_3$ peaks are significantly higher for the samples reacted in 1.5-M solutions when compared with samples treated in a 1.0-M solution. The difference in intensities upon adding the KOH mineralizer is not significant. The dependence on concentration is expected; however, substantial residual metallic Ti is present in all cases. No TiO_2 peaks are observed in the patterns; however, this does not rule out the existence of amorphous material. AFM images of the 250-nm thick Ti templates reacted in 1.0- and 1.5-M solutions for 5 h at 200 °C are given in Fig. 2. The morphology of the samples seen here is consistent with the XRD data and with the molarity dependence of grain morphology that has been reported by previous authors. Sample surface in Fig. 2(a) reveals a bimodal grain size distribution, while the sample surface in Fig. 2(b) shows grains whose average diameter is more uniform. This is consistent with a well-known behavior of hydrothermally derived $BaTiO_3$ films in which high pH and Ba^{2+} concentration favor $BaTiO_3$ crystallization reactions and a more homogeneous microstructure with smaller variations in grain size.[40]

Figure 3 shows XRD data related to $BaTiO_3$ formation on planar Ti films with different as-sputtered thicknesses.

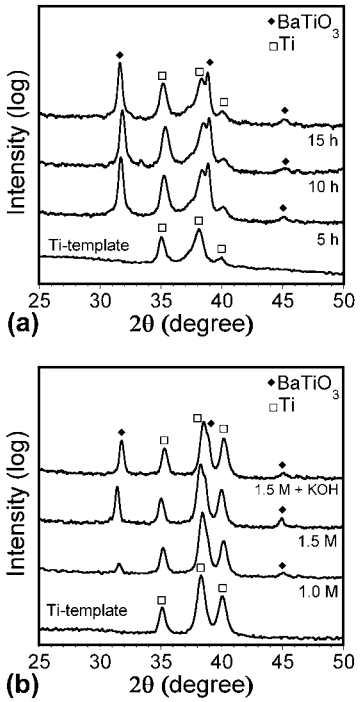


FIG. 1. X-ray diffraction patterns showing $BaTiO_3$ formation on Si substrates for (a) 250-nm thick planar Ti template as a function of time, 1.5 M, 200 °C and (b) 500-nm thick planar Ti template as a function of molarity, 5 h, 200 °C.

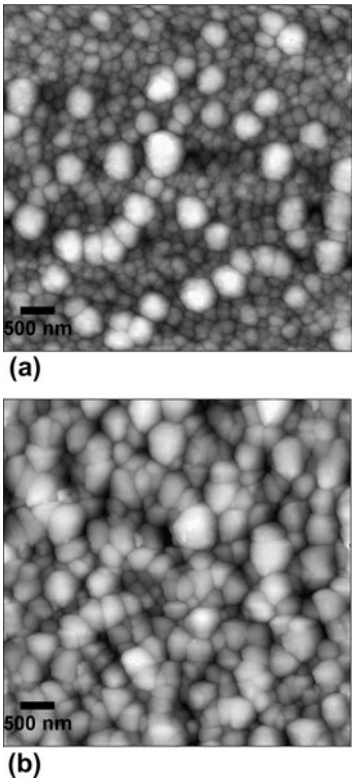


FIG. 2. Atomic force microscopy images of 250-nm thick planar Ti template treated for 5 h at 200 °C in solutions with the molarity of (a) 1.0 M and (b) 1.5 M.

https://doi.org/10.1557/jmr.2010.102 Published online by Cambridge University Press

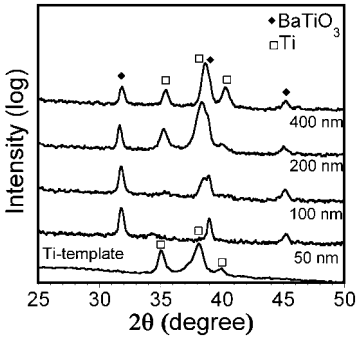


FIG. 3. $BaTiO_3$ formation on planar Ti templates with different thicknesses, 1.5 M solution, 5 h, 200 °C on Si substrate.

All films shown in Fig. 3 were reacted hydrothermally in a 1.5-M solution for 5 h at 200 °C. The pattern of a pure 250-nm thick Ti film is also given as a comparison. These data clearly demonstrate that the maximum thickness attained for the conversion of template to $BaTiO_3$ is not more than 100 nm under the current conditions. Similar thickness conversions were also reported in the literature on Ti and TiO_2 planar templates.[23,25,41] Further, it was reported that 0.25-mm thick Ti foils treated for 2 weeks at 240 °C could only yield a $BaTiO_3$ film of 500 nm thickness, and this thickness remained constant thereafter.[29] Therefore, there is a practical limit for the ultimate thickness of $BaTiO_3$ films prepared by reaction of planar Ti templates.

Overcoming this limitation is possible by engineering the morphology of the Ti template, and several authors have reported data suggesting this possibility.[33,42] Consequent to our observations of thickness limitations and the possibility of an engineered reactive template, we next explore the hydrothermal conversion of nanostructured Ti films.

B. Pillar templates

To gain control of growth rate, thickness, and final morphology of hydrothermally reacted $BaTiO_3$, we substituted a Ti layer comprising Ti nanopillars instead of using a flat Ti layer. XRD data and SEM surface image of the pillar-shaped Ti template are given in Figs. 4(a) and 4(b), respectively. This precursor layer was produced via collimated glancing angle sputter deposition in 2 h, under 1 mTorr Ar pressure.

Thickness measurements performed on the templates and the films after precipitation using profilometry showed that there is always an increase in film thickness around 90% in the out-of-plane direction. The accommodation of this dimensional change without mechanical failure is not possible for a flat Ti layer precursor. In case of pillar morphology, this complete conversion and volume change appears to be possible given the ability to transport solution between pillars and the ability of $BaTiO_3$ to grow laterally during conversion into the void space between individual precursor template pillars. XRD data show the formation of crystalline Ti, while the SEM image confirms that Ti is nucleating and growing on the substrate as a tilted random array of nanorods with a diameter of ~100 nm. These nanosculpted films were

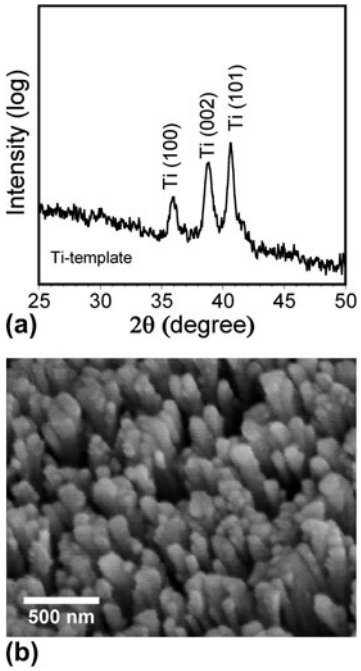


FIG. 4. (a) X-ray diffraction pattern and (b) plan view image of collimated glancing angle sputter-deposited Ti template on Si substrate.

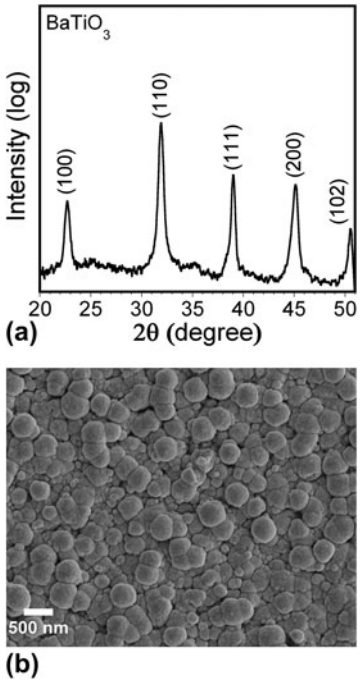


FIG. 5. (a) X-ray diffraction pattern and (b) plan view image of 650-nm thick $BaTiO_3$ film produced hydrothermally in 1.5-M solution for 2 h at 200 °C from pillar Ti templates on Si substrate.

https://doi.org/10.1557/jmr.2010.102 Published online by Cambridge University Press

treated in a 1.5-M solution at 200 °C for 2 h in a similar fashion as described for the planar templates in Fig. 1(b). Figure 5 shows XRD data and a representative surface SEM image of these templates after hydrothermal synthesis. According to XRD analysis, there is no unreacted Ti after hydrothermal conversion. In addition, the SEM image suggests a dense microstructure where the voids between the pillars have been filled by $BaTiO_3$ ceramic that formed by hydrothermal reaction, as hypothesized originally.

Figure 6(a) shows capacitance density and loss tangent as a function of frequency for $BaTiO_3$ film produced from ~350-nm thick pillar-shaped Ti template on platinized-Si substrate. In the as-precipitated state, the film exhibits a permittivity of ~1000 and loss tangent values around 10% at a test frequency of 100 kHz. A gradual decline of the permittivity observed here was attributed to the relaxation of polarization contributions from hydroxyl groups located in the $BaTiO_3$ film.[26,35] Dielectric loss behavior seen here also depends on the frequency-dependent reconfiguration of the hydroxyl groups, the time lag between the hydroxyl dipole switching, and space charges due to proton hopping.[14,35]

Annealing these films under forming gas containing 1 vol% H_2 for 3 h at 200 °C decreased both losses and the permittivity. This behavior is shown in Fig. 6(b). After annealing, the film exhibited a dielectric constant of ~900 and loss tangent values around 6% at 100 kHz frequency. This degree of loss reduction is observed commonly in hydrothermally derived $BaTiO_3$ films and is attributed to the removal of surface water and hydroxyl groups from the structure. Ambient atmosphere and pure oxygen-atmosphere annealing was also performed on the same samples at 200 °C and from 200 to 600 °C, respectively. Results, which are not reported here, show that the forming gas atmosphere is most effective to minimize dielectric loss. A similar dependence between loss tangent and annealing atmosphere was reported by McCormick and Slamovich[35] for hydrothermal $BaTiO_3$ samples treated under pure oxygen and Ar–5% H_2 atmosphere at 500 °C.

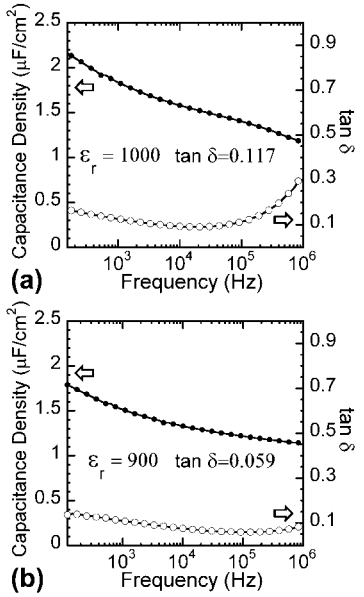


FIG. 6. Frequency dependence of capacitance density (solid markers) and loss tangent (open markers) for (a) as-precipitated 650-nm thick $BaTiO_3$ from pillar template, (b) as-annealed film under forming gas for 3 h at 200 °C. (Relative permittivity and tan δ values refer to measurements at a test frequency of 100 kHz.)

As discussed in the experimental section, Mn was added to a series of precursor solutions in an attempt to acceptor-dope the $BaTiO_3$. Mn was added by dissolving $MnCl_2 \cdot 4H_2O$ in distilled water and directly incorporating into the main $Ba(OH)_2$ solution prior to hydrothermal synthesis. The compositions produced are estimated by assuming that the solution concentration (cation ratio) is preserved in the final film. Figure 7 shows XRD patterns of this sample series, and the data reveal no secondary or manganese oxide phases, with only $BaTiO_3$ peaks present, consistent with the previous study on chemical solution–deposited Mn-doped $BaTiO_3$ films.[37]

The measurements of electrical properties of Mn-doped samples showed that the addition of the acceptor decreased both the permittivity and loss of the films in the as-precipitated state. For example, addition of 0.5 at.% Mn decreased the permittivity of the film from 1000 to 900 [Fig. 6(a)]. This reduction approached 50% when Mn content was increased to 2.0 at.%. In all cases of Mn-doped materials, loss tangent values fell below 0.1 and showed a minimum value around 0.08 with 2.0 at.% Mn addition. When Mn content was increased further, the permittivity and loss tangent values increased rapidly.

As in the undoped case, postdeposition/conversion anneals in air, oxygen, and forming gas atmospheres were explored. Again, in all cases, the forming gas anneals were most effective in minimizing dielectric loss. Figure 8 illustrates the representative example of frequency-dependent dielectric response for 1.0 at.% Mn-doped sample, up to 1 MHz for the as-precipitated state [Fig. 8(a)] and the as-annealed film [Fig. 8(b)]. Annealing was carried out under flowing forming gas containing 1.0 vol% H_2 balance N_2 at 200 °C, for 3 h. In comparison with the undoped case [shown in Fig. 6(b)], 1.0 at.% Mn

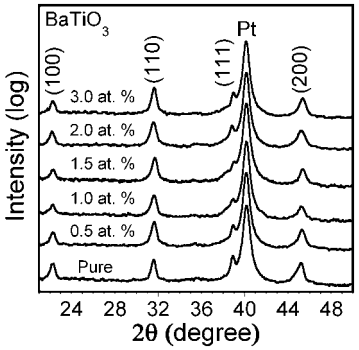


FIG. 7. X-ray diffraction patterns for pure and Mn-doped $BaTiO_3$ thin films on platinized-Si substrates.

https://doi.org/10.1557/jmr.2010.102 Published online by Cambridge University Press

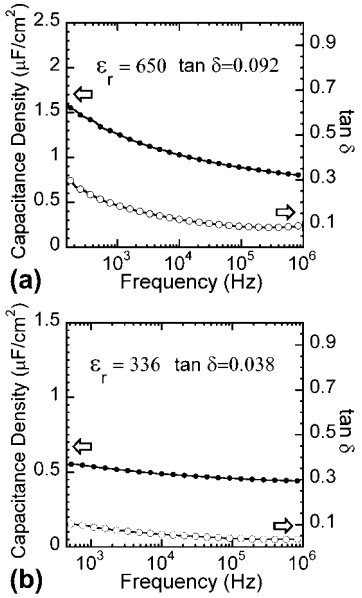


FIG. 8. Frequency dependence of capacitance density (solid markers) and loss tangent (open markers) for (a) 1.0 at.% Mn-doped as-precipitated $BaTiO_3$ thin film and (b) as-annealed film under forming gas for 3 h at 200 °C. (Relative permittivity and tan δ values refer to measurements at a test frequency of 100 kHz.)

incorporation decreases the frequency dependence of both capacitance and loss tangent at radio frequencies. This sample exhibits a loss tangent value of 0.038 at 100 kHz. Ultimately, addition of 0.072 g of $MnCl_2 \cdot 4H_2O$ into the solution, which yields 1:100 for Mn:Ba ion ratio, during hydrothermal treatment is sufficient to reduce loss tangents below 10% over the entire measurement range.

With these findings in mind, we propose the following mechanism to describe the apparent ability of forming gas annealing and Mn-doping to produce low loss tangent values in hydrothermal $BaTiO_3$.

Chien et al.[14] identified a set of three physical mechanisms by which the hydroxide defects that populate hydrothermal $BaTiO_3$ are eliminated. The three stages, which occur subsequently with increasing temperature, are given by the following equations and their roughly associated temperature regimes:

$$\text{Regime I}: (\text{RT to } 200\,^{\circ}\text{C})$$

$$H_2O_{(surface)} \Rightarrow H_2O_{(g)}\uparrow$$

$$\text{Regime II}: (200 - 800\,^{\circ}\text{C})$$

$$2OH_O^{\bullet} + V_{Ba}^{//} \Rightarrow H_2O_{(g)}\uparrow + V_O^{\bullet\bullet} + V_{Ba}^{//} + O_O^X \,(ionic)$$
$$2OH_O^{\bullet} + 2e^- \Rightarrow H_2O_{(g)}\uparrow + V_O^{\bullet\bullet} + 2e^- + O_O^X \,(electronic)$$

$$\text{Regime III}: (800\,^{\circ}\text{C and higher})$$

$$V_{Ba}^{//} + V_O^{\bullet\bullet} \Rightarrow nil\,(ionic)$$
$$V_O^{\bullet\bullet} + 2e^- + \frac{1}{2}O_2(g) \Rightarrow nil\,(electronic)$$

The removal of surface water and lattice hydroxides was observed via the evolution of water vapor and the creation of vacant anion sites. In regimes I and II, electroneutrality is most likely maintained by charge balance between a combination of positive hydroxyl species, negative metal vacancies, and electrons both before and after hydroxide loss. The existence of protons, vacancies, and electronic carriers contribute collectively to the high dielectric loss values that are observed routinely, and their elimination is consistent with the reduction of loss tangents and dispersion as annealing temperatures are increased. The fraction of electronic compensation must be substantial to explain the very high losses in hydrothermal $BaTiO_3$ at room temperature in which proton and vacancy diffusion is too slow to follow radio frequency fields.

We can understand our observations of reduced dielectric loss with annealing at 200 °C and lower still by annealing in forming gas as follows: (i) low-temperature annealing drives off surface water and decomposes some hydroxyl groups, and (ii) forming gas annealing enhances this process since the low pO_2 will thermodynamically favor the oxygen-vacancy formation that accompanies hydroxyl transformation to a water vapor product. At such low temperatures, this effect is not expected to be predominant, and thus it is consistent with the modest but reproducibly lower loss tangents observed after forming gas as opposed to oxygen annealing. In comparison, for oxygen gas annealing, it was very difficult to find any capacitors in which loss tangent values were less than 0.1 at any frequency.

Finally, we are left to explain the impact of Mn-doping. The first consideration along these lines is the nature of incorporation. In a recent study, Tong et al.[43] found that Mn ions are found in the form of Mn^{2+} in hydrothermally produced Mn-doped $BaTiO_3$ nanoparticles. If we assume similar behavior in our thin-film system, we can propose the following defect chemical reactions taking place in annealing temperature regime II:

$$\text{Regime II with Mn} - \text{doping}: (200 - 800\,^{\circ}\text{C})$$

$$2OH_O^{\bullet} + Mn_{Ti}^{//} \Rightarrow H_2O_{(g)}\uparrow + V_O^{\bullet\bullet} + Mn_{Ti}^{//}\,(extrinsic)$$

This doping will compete with the intrinsic mechanisms to compensate for aliovalent hydroxide ions. Most importantly, Mn-doping will substantially reduce the number of electronic charge carriers (as is well known for low pO_2 sintered $BaTiO_3$) and can produce the lower loss tangent and frequency dispersion values we observe.

https://doi.org/10.1557/jmr.2010.102 Published online by Cambridge University Press

Finally, we must explain the reduction in permittivity that accompanies Mn incorporation. Such behavior has been seen by other authors[44–48] and has been attributed to the ability of aliovalent dopants to pin the motion of domain walls. Mn substitution (especially the 2+ valence state) presents a substantial charge discontinuity that will interfere with the 180° wall motion that leads to high permittivity under small signal measurements. This effect is analogous to aging in piezoelectric ceramic capacitors.[49] It is important to note that though textured templates and acceptor doping are effective in improving microstructure and reducing loss tangents, additional research is needed to improve breakdown strength. The yield for dot capacitors produced by this method was greater than 75%; however, the films could not withstand electric fields much greater than 60 kV/cm without exhibiting uncontrolled loss tangents.

IV. SUMMARY

$BaTiO_3$ thin films were produced via hydrothermal reaction. Sputter-deposited Ti films on Si or platinized-Si substrates and $Ba(OH)_2$ solution were used as precursors. Templates were prepared in two morphologies, i.e., planar and pillar. Samples were treated at 200 °C for a variety of Ba concentrations and durations. The samples produced from flat templates showed sluggish transformation kinetics and an eventual termination of reaction without fully consuming the Ti metal. Templates with pillar morphology, on the other hand, could be transformed to phase-pure $BaTiO_3$ independent of the template thickness. Optimum conditions for the transformation were found as 2 h, 1.5 M, and 200 °C. The films revealed a high dielectric constant and losses around 10% in as-precipitated state. Annealing these films under forming gas containing 1 vol% H_2 for 3 h at 200 °C decreased high-field losses to 0.06 and the dependence of permittivity to frequency. Mn as an acceptor dopant improved dielectric properties of the films up to 2.0 at.% and acted as a supporting mechanism to reduce the overall defect concentration. Annealing of doped-samples at just 200 °C under forming gas containing 1 vol% H_2 for 3 h completely eliminated the frequency dispersion of both the permittivity and tangent loss. The study demonstrates that nanostructuring and designing the precursor layer provides control on the net diffusion direction and eliminates the need for long-range transport. Finally, though some annealing was needed to achieve low loss tangent values, the maximum temperatures were within the survivability range of several polymer package materials.

ACKNOWLEDGMENTS

Financial support for Hasan Akyıldız was provided by TUBITAK-BIDEP and by NSF (contract 0547134); both are gratefully acknowledged.

REFERENCES

1. D. Henning, M. Klee, and R. Waser: Advanced dielectrics: Bulk ceramics and thin films. *Adv. Mater.***3**(7/8), 334 (1991).
2. A.S. Bhalla, R. Guo, and R. Roy: The perovskite structure-a review of its role in ceramic science and technology. *Mater. Res. Innovations* **4**, 3 (2000).
3. B.S. Kwak, K. Zhang, E.P. Boyd, A. Erbil, and B.J. Wilkens: Metalorganic chemical vapor deposition of $BaTiO_3$ thin films. *J. Appl. Phys.* **69**(2), 767 (1991).
4. J.P. Chu, T. Mahalingam, C.F. Liu, and S.F. Wang: Preparation and characterization of Mn-doped $BaTiO_3$ thin films by magnetron sputtering. *J. Mater. Sci.* **42**, 346 (2007).
5. R. Kullmer: Dielectric and ferroelectric properties of pulsed-laser deposited $BaTiO_3$ films. *Appl. Phys.Mater. Sci. Process.* **65**, 273 (1997).
6. C.T. Wu and F.H. Lu: Electrochemical deposition of barium titanate films using a wide electrolytic range. *Thin Solid Films*. **398–399**, 621 (2001).
7. H.B. Sharma and H.N.K. Sarma: Electrical properties of sol-gel processed barium titanate films. *Thin Solid Films*. **330**, 178 (1998).
8. N. Golego, S.A. Studenikin, and M. Cocivera: Properties of dielectric $BaTiO_3$ thin films prepared by spray pyrolysis. *Chem. Mater.* **10**, 2000 (1998).
9. J. Ihlefeld and B. Laughlin: A. H-Lowery, W. Borland, and J.-P. Maria: Copper compatible barium titanate thin films for embedded passives. *J. Electroceram.* **14**, 95 (2005).
10. P.-H. Chan and F.-H. Lu: Low-temperature hydrothermal-galvanic couple synthesis of $BaTiO_3$ thin films on Ti-coated silicon substrates. *Thin Solid Films*. **517**, 4782 (2009).
11. P.M. Raj, D. Balaraman, I.R. Abothu, C. Yoon, N.-K. Kang, and R. Tummala: Integrating high-k ceramic thin film capacitors into organic substrates via low-cost solution processing. *IEEE Trans. Compon. Packag. Technol*. **30**(4), 585 (2007).
12. N. Ishizawa, H. Banno, M. Hayashi, S.E. Yoo, and M. Yoshimura: Preparation of $BaTiO_3$ and $SrTiO_3$ polycrystalline thin films on flexible polymer film substrate by hydrothermal method. *Jpn. J. Appl. Phys.* **29**(11), 2467 (1990).
13. E.B. Slamovich and I.A. Aksay: Structure evolution in hydrothermally processed (<100 °C) $BaTiO_3$ films. *J. Am. Ceram. Soc.* **79** (1), 239 (1996).
14. A.T. Chien, X. Xu, J.H. Kim, J. Sachleben, J.S. Speck, and F.F. Lange: Electrical characterization of $BaTiO_3$ heteroepitaxial thin films by hydrothermal synthesis. *J. Mater. Res.* **14**(8), 3330 (1999).
15. D. Balaraman, P.M. Raj, L. Wan, I.R. Abothu, S. Bhattacharya, S. Dalmia, M.J. Lance, M. Swaminathan, M.D. Sacks, and R.R. Tummala: $BaTiO_3$ films by low-temperature hydrothermal techniques for next generation packaging applications. *J. Electroceram.* **13**, 95 (2004).
16. R.Z. Hou, A. Wu, and P.M. Vilarinho: Low-temperature hydrothermal deposition of $(Ba_xSr_{1-x})TiO_3$ thin films on flexible polymeric substrates for embedded applications. *Chem. Mater.* **21**, 1214 (2009).
17. R.R. Bacsa, J.P. Dougherty, and L.J. Pilione: Low-temperature synthesis of $BaTiO_3$ thin films on silicon substrates by hydrothermal reaction. *Appl. Phys. Lett.* **63**(8), 1053 (1993).
18. M.E. Pilleux and V.M. Fuenzalida: Hydrothermal $BaTiO_3$ films on silicon: Morphological and chemical characterization. *J. Appl. Phys.* **74**(7), 4664 (1993).
19. E. Shi, C.-R. Cho, M.-S. Jang, S.-Y. Jeong, and H.J. Kim: The formation mechanism of barium titanate thin film under hydrothermal conditions. *J. Mater. Res.* **9**(11), 2914 (1994).
20. C.-R. Cho, E. Shi, M.-S. Jang, S.-Y. Jeong, and S.-C. Kim: Structural and electrical properties of $BaTiO_3$ thin films on Si (100) substrate by hydrothermal synthesis. *Jpn. J. Appl. Phys.* **33**, 4984 (1994).

https://doi.org/10.1557/jmr.2010.102 Published online by Cambridge University Press

21. C.R. Cho, M.S. Jang, S.Y. Jeong, S.J. Lee, and B.M. Lim: Ferroelectric properties of hydrothermally prepared $BaTiO_3$ thin films on Si(100) substrates by low-temperature processing. *Mater. Lett.* **23**, 203 (1995).
22. W. Xu, L. Zheng, H. Xin, C. Lin, and M. Okuyama: Hydrothermal $BaTiO_3$ thin films on Ti-covered silicon: Characterization and growth mechanism. *J. Electrochem. Soc.* **143**(3), 1133 (1996).
23. V.M. Fuenzalida, M.E. Pilleux, and I. Eisele: Adsorbed water on hydrothermal $BaTiO_3$ films: Work function measurements. *Vacuum*. **55**, 81 (1999).
24. K.W. Seo and H.G. Kong: Hydrothermal preparation of BaTiO3 thin films. *Korean*. *J. Chem. Eng.* **17**(4), 428 (2000).
25. T. Hoffmann, T. Doll, and V.M. Fuenzalida: Fabrication of $BaTiO_3$ microstructures by hydrothermal growth. *J. Electrochem. Soc.* **144**(11), L292 (1997).
26. C.K. Tan, G.K.L. Goh, D.Z. Chi, A.C.W. Lu, and B.K. Lok: Hydrothermal growth of $BaTiO_3$ thin films on printed circuit boards for integral capacitor applications. *J. Electroceram.* **16**, 581 (2006).
27. K. Kajiyoshi, N. Ishizawa, and M. Yoshimura: Preparation of tetragonal barium titanate thin film on titanium metal substrate by hydrothermal method. *J. Am. Ceram. Soc.* **74**(2), 369 (1991).
28. R. Bacsa, P. Ravindranathan, and J.P. Dougherty: Electrochemical, hydrothermal, and electrochemical-hydrothermal synthesis of barium titanate thin films on titanium substrates. *J. Mater. Res.* **7**(2), 423 (1992).
29. W. Zhu, S.A. Akbar, R. Asiaie, and P.K. Dutta: Synthesis, microstructure and electrical properties of hydrothermally prepared ferroelectric $BaTiO_3$ thin films. *J. Electroceram.* **2**(1), 21 (1998).
30. J.G. Lisoni, F.J. Piera, M. Sánchez, C.F. Soto, and V.M. Fuenzalida: Water incorporation in $BaTiO_3$ films grown under hydrothermal conditions. *Appl. Surf. Sci.* **134**, 225 (1998).
31. W.-P. Xu, L. Zheng, C. Lin, and M. Okuyama: Mild hydrothermal synthesis of titanate films: From polycrystalline $BaTiO_3$ to epitaxial $PbTiO_3$. *Philos. Mag. B*. **77**(1), 177 (1998).
32. J. Xu, J. Zhai, and X. Yao: Structure and dielectric nonlinear characteristics of $BaTiO_3$ thin films prepared by low temperature process. *J. Alloy. Comp.* **467**, 567 (2009).
33. X. Wei: Hydrothermal synthesis of $BaTiO_3$ thin films on nanoporous TiO_2 covered Ti substrates. *J. Cryst. Growth*. **286**, 371 (2006).
34. C.K. Tan and G.K.L. Goh: Growth and dielectric properties of solvothermal $BaTiO_3$ polycrystalline thin films. *Thin Solid Films*. **515**, 6572 (2007).
35. M.A. McCormick and E.B. Slamovich: Microstructure development and dielectric properties of hydrothermal $BaTiO_3$ thin films. *J. Eur. Ceram. Soc.* **23**, 2143 (2003).
36. F.F. Lange and G.K.L. Goh: Hydrothermal epitaxial growth of perovskite films. *J. Cer. Proc. Res.* **2**(1), 4 (2001).
37. J.F. Ihlefeld, M.D. Losego, R. Collazo, W.J. Borland, and J.-P. Maria: Defect chemistry of nano-grained barium titanate films. *J. Mater. Sci.* **43**, 38 (2008).
38. M. Dong, H. Miao, G. Tan, and Y. Pu: Effects of Mg-doping on the microstructure and properties of $BaTiO_3$ ceramics prepared by hydrothermal method. *J. Electroceram.* **21**, 573 (2008).
39. B. Dick, M.J. Brett, T. Smy, M. Belov, and M.R. Freeman: Periodic submicrometer structures by sputtering. *J. Vac. Sci. Technol. B*. **19** (5), 1813 (2001).
40. K.-M. Hung, C.-S. Hsieh, W.-D. Yang, and Y.-J. Sun: The prepatory optimal conditions of barium titanate thin film from a hydrothermal method at low temperature. *J. Mater. Sci.* **42**, 2376 (2007).
41. W.-P. Xu, L. Zheng, C. Lin, and M. Okuyama: (111)-Oriented $BaTiO_3$ thin films hydrothermally formed on TiO_2/Si substrate. lntegr. *Ferroelectr.* **12**, 233 (1996).
42. Y. Li, X.P. Gao, G.R. Li, G.L. Pan, T.Y. Yan, and H.Y. Zhu: Titanate nanofiber reactivity: Fabrication of $MTiO_3$ (M=Ca, Sr, and Ba) perovskite oxides. *J. Phys. Chem. C*. **113**, 4386 (2009).
43. X. Tong, Y.-H. Lin, S. Zhang, Y. Wang, and C.-W. Nan: Preparation of Mn-doped $BaTiO_3$ nanoparticles and their magnetic properties. *J. Appl. Phys.* **104**, 066108 (2008).
44. J.F. Ihlefeld: Synthesis and properties of barium titanate solid solution thin films on copper substrates. Ph.D. Thesis, North Carolina State University, (2006).
45. Y. Li, X. Yao, X. Wang, and L. Zhang: Studies of resistivity and dielectric properties of manganese-doped barium titanate sintered in pure nitrogen. *Ferroelectrics*. **384**, 73 (2009).
46. S.-F. Wang, Y.-C. Hsu, J.P. Chu, and C.-H. Wu: Hexagonal $Ba(Ti_{1-x}Mn_x)O_3$ ceramics: Microstructural evolution and microwave dielectric properties. *Appl. Phys. Lett.* **88**, 042909 (2006).
47. T. Li, L. Li, J. Zhao, and Z. Gui: Modulation effect of Mn^{2+} on dielectric properties of $BaTiO_3$-based X7R materials. *Mater. Lett.* **44**, 1 (2000).
48. J. Tangsritrakul, M. Unruan, P. Ketsuwan, and R. Yimnirun: Effects of manganese addition on the phase formation, microstructure, and electrical properties of barium titanate ceramics. *Adv. Mat. Res.* **55–57**, 97 (2008).
49. A.J. Moulson and J.M. Herbert: *Electroceramics: Materials-Properties-Applications* (John Wiley & Sons Press, England, 2003), p. 357.

https://doi.org/10.1557/jmr.2010.102 Published online by Cambridge University Press